Electronic Supplementary Material (ESI) for ChemComm.
This journal is © The Royal Society of Chemistry 2019

Electronic Supplementary Information

Selective Synthesis of Single Layer Translucent Cobalt Hydroxide for Efficient Oxygen Evolution Reaction

Priyajit Jash[a], Pradhi Srivastava[b], and Amit Paul*[a]

[a]Department of Chemistry

[b]Department of Electrical Engineering & Computer Science

IISER Bhopal, Bhopal 462066, MP, India

Email address for correspondence: apaul@iiserb.ac.in

Page no.	Contents
S2-S3	Chemicals, materials synthesis
S3-S4	Materials characterization
S4-S6	Electrochemical measurements
S6-S7	BET results, SEM and AFM images, Tyndall effect
S7-S9	Activity parameter, ECSA, RF calculation methodology
S9-S10	AC Impedance results, Equivalent circuit fitted parameters and AC Impedance discussion
S11	23 hour Chronoamperometry and O_2 detection
S11	Post catalysis morphology (TEM and SEM)
S12	EDAX spectrum, elemental mapping before and after electrocatalysis
S13	Literature reports of recently studied cobalt hydroxide water oxidation electrocatalysts
S13	References

Experimental Section:

Chemicals:

Cobalt chloride ($CoCl_2 \cdot 6H_2O$), hexamethylenetetramine (HMT), sodium nitrate ($NaNO_3$), formamide (99.6%), and Nafion perfluorinated resin solution were purchased from Sigma-Aldrich. Sodium chloride (NaCl) and sodium hydroxide (NaOH) were purchased from S D Fine-Chem. Ltd, India and Emplura respectively. Isopropyl alcohol and ethanol were obtained from Ranchem Pvt. Ltd. Inductively coupled plasma (ICP) graded HNO_3 was purchased from Merck. Millipore Milli-Q water (resistivity ~18.2 MΩ.cm) was used throughout the study.

Material synthesis:

Synthesis of α-$Co(OH)_2$ and β-$Co(OH)_2$:

In a typical synthesis of **α-$Co(OH)_2$**, 10 mM of $CoCl_2 \cdot 6H_2O$, 50 mM of NaCl and 60 mM of HMT were mixed in 200 ml (9:1) de-ionized (DI) water and ethanol mixture. The reaction mixture was heated at 90 °C for 1 h under magnetic stirring. Then the solution was cooled down to room temperature and the resultant solid green powder was filtered. Subsequently, the green powder was washed several times with DI water and ethanol and finally vacuum dried at room temperature. The synthesis procedure of **β-$Co(OH)_2$** was same except the concentration of $CoCl_2 \cdot 6H_2O$ was reduced to 5 mM without the addition of NaCl. Both the products were confirmed as α and β phases respectively through powder XRD analysis.

Synthesis of SL-$Co(OH)_2$ (SL suggests single layer):

The as synthesized **α-$Co(OH)_2$** sample (25 mg) was dispersed in 20 ml of ethanol/water (1:1 v/v) binary solution of 1 M $NaNO_3$. The mixture was then mechanically stirred under continuous N_2 flow for 24 h. The exchanged products were separated using the same

procedure described for the pristine material. After that, 5.48 mg of that sample was dispersed in 12 ml of degased formamide by 5 min sonication and mechanically stirred under N_2 atmosphere for 24 h. A reddish translucent colloidal suspension was formed. For the purification purpose of the exfoliated product, the resulting solution was centrifuged at 6000 rpm for 10 min. Our results indicated that there was almost no non exfoliated residue remaining at the bottom of the centrifuge tube. Thus the exfoliation harvest was nearly 100%. We have further confirmed that the exfoliation product as **SL-Co(OH)$_2$** by irradiating with laser beam which displayed the tyndall effect.

Materials Characterization:

High angle powder X-ray diffraction (XRD) of all the materials were carried out in the region 5-70° using PANalytical EMPYREAN diffractometer with Cu Kα radiation (λ = 1.54 Å). For N_2 adsorption-desorption experiments, samples were heat-treated at 100 °C for 24 h in vacuum followed by sorption analyses at –196 °C using an AutosorbiQ Station 1 after degassing at 100 °C for 12 h under vacuum. The surface area and pore size distribution were estimated by multipoint Brunauer–Emmett–Teller (BET) and nonlocal density functional theory (NLDFT) method, respectively. For transmission electron microscopy (TEM), powder samples were dispersed in isopropanol and one droplet of the suspension was deposited on carbon coated Cu mesh 200 grid, dried in vacuum, and analysed by FEI TALOS200S at 200 kV operating voltage. Field emission scanning electron microscopy (FESEM) images of the samples were collected using Carl Zeiss (ultraplus) equipment with an energy dispersive spectrometer of Oxford Instruments X-MaxN at a working voltage 20 kV. Energy dispersive X-ray spectroscopy (EDS) and elemental mapping experiments were performed using a spectrometer (Oxford Instruments X-Max) attached to SEM. For the exfoliated **SL-Co(OH)$_2$,** one droplet of the colloidal solution was directly deposited on the Cu grid. The content of cobalt in all the prepared samples were determined by digesting very small quantity of these

samples to 25 ml savillex teflon pressure decomposition vessels by dissolving in $HCl:HNO_3$ (3:1 v/v) solutions. After overnight digestion, it was diluted 10 times prior to high resolution inductively coupled plasma optical emission spectrometry (ICP-OES) instrument (Agilent TechnologiesModel: 725). Atomic force microscopy (AFM) was performed on an Agilent Technologies, Model No.-5500 (Agilent Technologies Santa Clara, California, United States) instrument in tapping mode. Rectangular cantilevers with approximate dimensions of 125 mm in length and 40 mm in width (µmasch Sensor NSC 15) were used to perform the tapping mode experiments. The sample was prepared by dispersing the colloidal solution on silicon substrates for 10 min. After that by washing with DI water, it was dried at 125 °C for 10 min in oven. The Pico View software (version 1.10, Agilent) was used to analyse the recorded AFM data.

Electrochemical measurements:

For electrochemical experiments, first glassy carbon (GC) electrode (geometrical area = 0.07 cm^2, diameter 3 mm) was mechanically polished by using 0.05 micron sized alumina powder to mirror finish. Then, 1.2 mg of catalyst was dispersed in a mixture of Nafion per fluorinated resin solution (12.5 µL) and water/isopropyl alcohol (250 µL, 3:1 v/v). After homogeneous dispersion by sonication, an aliquot (1 µL) was drop casted on the GC electrode, and the electrode was then dried at 70 °C for 30 min to evaporate the solvents, leading to a catalyst loading of 0.065 mg cm^{-2}. However for the **SL-Co(OH)$_2$**,10 µL of the colloidal solution directly deposited on the glassy carbon keeping the same amount of loading 0.065 mg cm^{-2} and heated at 125 °C for 10 min. The electrochemical experiments were carried out in 1 M aq. NaOH solution (pH 13.9) consisting of GC, Ag/AgCl (3M KCl) electrode, and Pt wire as working, reference, and counter electrodes, respectively at 25 °C. CH Instruments, Austin, TX (CHI 760D) were used for all the electrochemical experiments. Cyclic voltammetry (CV) experiments were performed at a scan rate of 5 mVs^{-1} while the solution was stirred at 1600

rpm to avoid O_2 bubbles accumulation near the electrode surface. A slow scan rate was chosen so that steady state can be achieved. The electrochemical results reported in this work were *IR* compensation corrected and potentials were reported with respect to the reversible hydrogen electrode (RHE) system by following the equation *E* (*vs.* RHE) = *E* (*vs.* Ag/AgCl) + 0.197 + 0.059 pH.[1] Electrochemical impedance spectroscopy (EIS) spectra were taken in the frequency range of 10^5 to 10^{-2} Hz at 1.58 V vs. RHE potential with amplitude of 5 mV. For the determination of ECSA, CVs were taken in the non-Faradaic zone (-0.05 to +0.05 V vs. Ag/AgCl reference electrode) without stirring the solutions at different scan rates. For the long-term stability test, the potential of the electrode was held at 1.58 V vs. RHE for 23 h. Chronoamperometry experiments were performed by stirring the electrolyte solution at 1600 rpm in order to make the solution free from in-situ generated oxygen bubble. Turnover frequencies (TOF), mass activities, and specific activities of all the catalysts were estimated from following Eqs. S1, S2 and S3.[2]

$$\text{TOF} = \frac{j * S_{geo}}{4 * F * n} \qquad \text{(S1)}$$

$$\text{Mass activity} = \frac{j}{m} \qquad \text{(S2)}$$

$$\text{Specific activity} = \frac{j}{S_{BET} * m} \qquad \text{(S3)}$$

In these equations, j, S_{geo}, S_{BET}, F, m, and n represent current density (mA/cm^2), geometrical surface area of electrode (cm^2), BET surface area (m^2 g^{-1}) from N_2 sorption analysis, Faraday constant (96485 C mol^{-1}), mass density (mg cm^{-2}) and moles of the catalyst, respectively. Mole quantification of each catalyst was done by estimating atomic weight of cobalt and nickel through inductively coupled plasma mass spectrometry (ICP-OES).

Oxygen-quantification and Faradic efficiency:

A HI 764080 Digital polarographic dissolved oxygen probe was chosen to measure the change of dissolved oxygen concentration in 1M NaOH solution kept in a four-mouth sealed electrode cell during control potential electrolysis (CPE). The experiments have been carried out by holding the GC electrode potential at 1.58 V (*vs*. RHE) to 30 min for **SL-Co(OH)$_2$** . Before performing the chronoamperometry experiment, the sensor was calibrated by using two points against solution and air while 1M NaOH solution was purged with Ar gas until the probe sensor showed zero O_2 concentration. The Faradaic efficiency was calculated from the total amount of charge (Q, C) passed through the cell and the total amount of the produced O_2 n_{O2} (mol). Faradaic efficiency = $4F*n_{O2}/Q$, wherein F is the Faraday constant, considering that the four electrons are needed to produce one oxygen molecule.

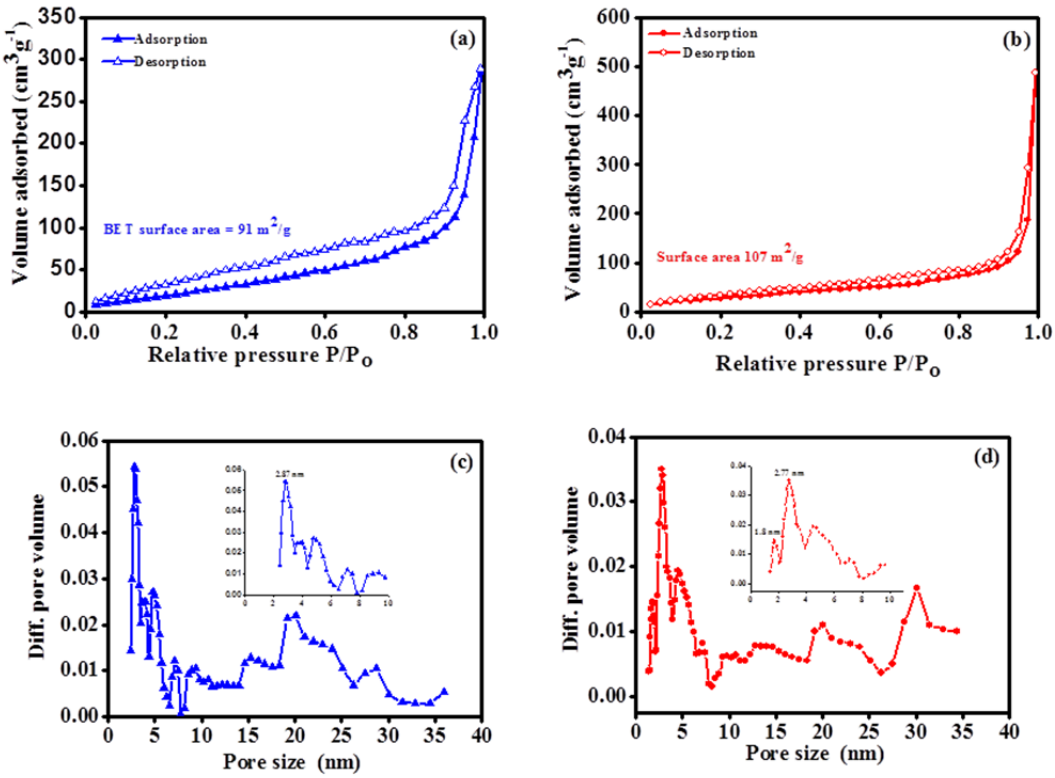

Figure S1: BET adsorption-desorption isotherm profiles (a-b) and the corresponding pore size distribution estimated by NLDFT method (c-d) for **β-Co(OH)$_2$** and **α-Co(OH)$_2$** respectively.

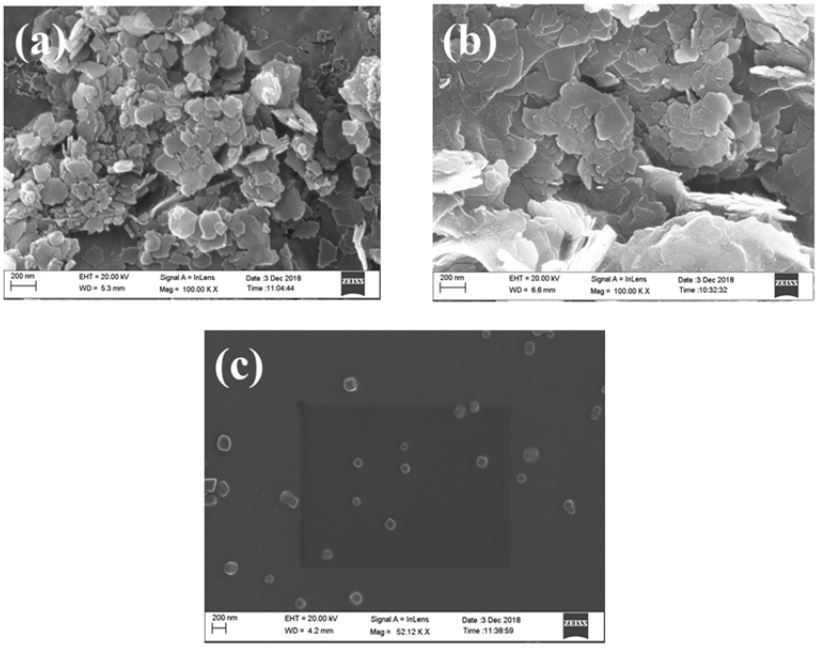

Figure S2: SEM images (a-c) **β-Co(OH)$_2$, α-Co(OH)$_2$** and **SL-Co(OH)$_2$** respectively (scale bar 200 nm)

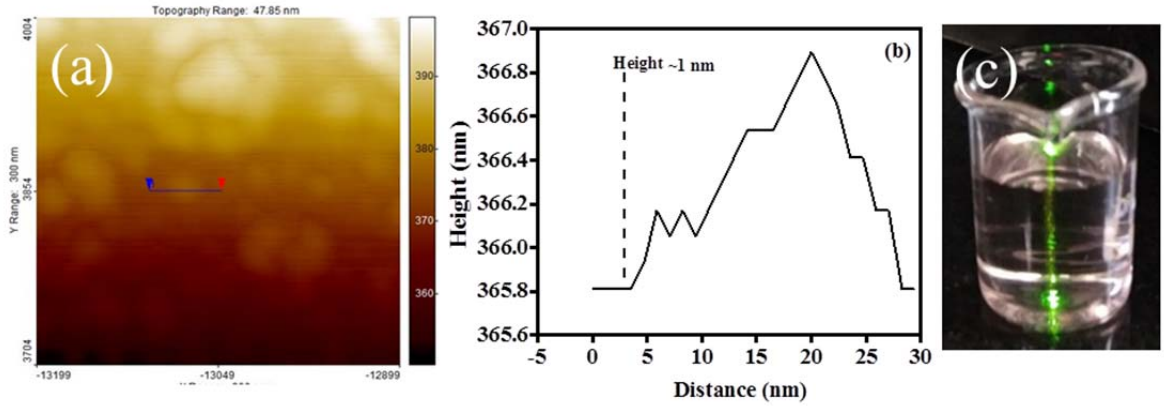

Figure S3: (a) Tapping-mode AFM image of exfoliated **SL-Co(OH)$_2$** on silicon wafer (b) corresponding height profile and (c) Visible tyndall effect when irradiated with laser beam.

Table S1: TOF, Mass and specific activities of all nanomaterials during electrocatalysis

Materials	TOF (s^{-1})	Mass activity @η=350 (j/m; A/g)	Specific activity @η=350 (j/S_{BET}*m; mA/cm^2)
SL-Co(OH)$_2$	0.146	153.8	-
α-Co(OH)$_2$	0.015	40.83	0.381
β-Co(OH)$_2$	0.003	9.47	0.104

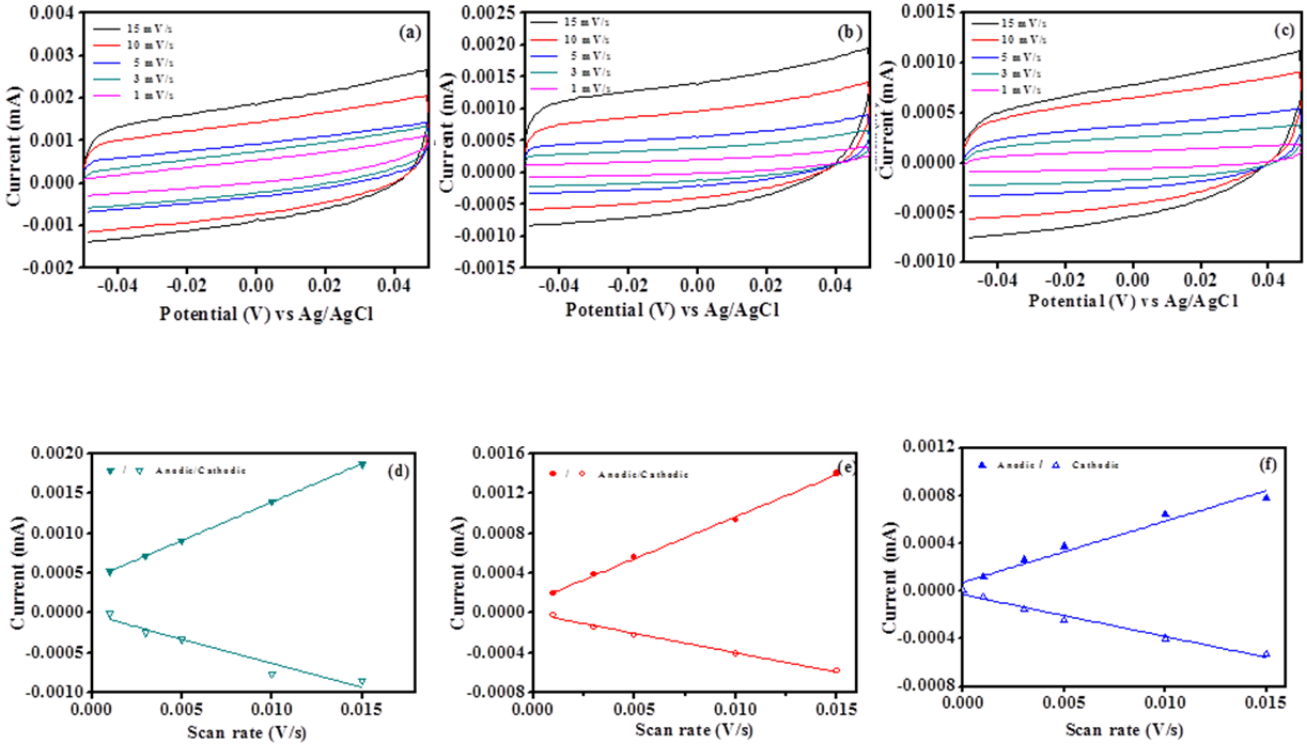

Figure S4: (a-c) CVs and (d-f) corresponding plots of anodic and cathodic charging currents at 0 V (potential region: -0.05-0.05 V *versus* Ag/AgCl) of **SL-Co(OH)$_2$, α-Co(OH)$_2$** and **β-Co(OH)$_2$** respectively.

Calculation of areal capacitance (C_{dl}, μF/cm^2), electrochemically accessible surface area (ECSA) and roughness factor (RF)

The charging current for cathodic (i_c) and anodic (i_a) currents were measured at 0 V *versus* Ag/AgCl. The relation between i_c/i_a *versus* scan rate (ν) and the double layer capacitance (C) were given by equations S4 (a-b).

$$i_a = \nu C \quad \text{..... (S4a)}$$

$$i_c = \nu C \quad \text{..... (S4b)}$$

The slopes of i_c and i_a as a function of ν provided *C* from the slope. The average slope calculated from cathodic and anodic currents was chosen as *C*. The geometrical area of the electrode (GSA) was 0.07 cm^2. The areal capacitances (C_{dl}, μF/cm^2) were calculated by dividing *C* with GSA. For the calculation of electrochemically accessible surface area (ECSA), equation S5 has been used wherein C_s=27 μF/cm^2 (specific surface area) taken from the literature.[3]

ECSA= C/C_S …… (S5)
Roughness factor (RF) was estimated using eq. S6.

Roughness Factor (RF) = ECSA/GSA ……. (S6)

Table S2: Non-faradic capacitances (C_{dl}), electrochemically accessible surface areas (ECSA), and surface roughness factors (RF) of nanomaterials.

Sample	Capacitance C_{dl} (μFcm^{-2})	ECSA (cm^2)	Roughness Factor (RF)
SL-Co(OH)$_2$	78.2	2.89	41.3
α-Co(OH)$_2$	61.5	2.27	32.5
β-Co(OH)$_2$	42.0	1.55	22.2

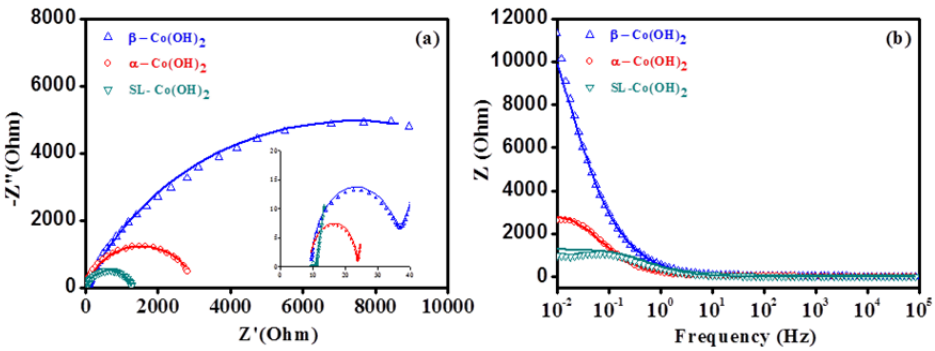

Figure S5: EIS measurements (a) Nyquist and (b) Bode plots of all the nanomaterial at 1.58 V *(vs.* RHE) in the frequency range from 10^5 to 10^{-2} s^{-1} with 0.005 V amplitude. The experimental results are represented by discrete points and equivalent circuit fitted results are represented by solid lines.

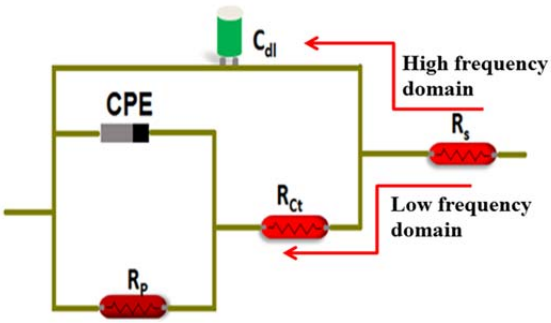

Figure S6: Equivalent circuit model used for fitting of OER catalysis. R_s, C_{dl}, R_{ct}, R_p, and CPE represent uncompensated solution resistance, double layer charging at the high frequency domain, charge transfer resistance at the electrode-electrolyte interface related to the overall OER, pseudoresistance which is related with one or more surface intermediates formation, and pseudocapacitance which represents change in charged surface species as OER proceeds respectively.

Electrochemical impedance spectroscopy (EIS):

All the EIS results were fitted using an equivalent circuit shown in Figure S5 wherein R_s, C_{dl}, R_{ct}, R_p, and CPE represent uncompensated solution resistance, double layer capacitance at the electrode-electrolyte interface at short time scale, charge transfer resistance at the electrode-electrolyte interface related to the overall OER, pseudoresistance which is related with one or more surface intermediates formation, and pseudocapacitance which represents change in charged surface species as OER proceeds. CPE is a constant phase element which is often used in lieu of a capacitor that arises due to inhomogeneity in charge dispersion and defined as $Z_{CPE} = CPE^{-1}(i\omega)^{-\alpha}$ wherein α varies between 0 to 1.[4] The R_p-CPE loop reflects the relaxation of charge associated with the surface intermediates formation and dictates the second semicircle formation in the low frequency region.[5] It is important to highlight, at the higher frequencies, owing to the short timescale, the ion penetration deep inside the nanomaterial drops out.[6] As soon as frequency progress towards the intermediate frequency, more quantity of charge was stored inside nanomaterial which was reflected in the CPE values. The capacitance values in CPE were in the milifarad range whereas the double layer capacitance (C_{dl}) values are in the micro farad range which was very less attributing the less amount of charge accumulation during the short span of physical process.

Table S3: Equivalent circuit parameters calculated from EIS fitting for all nanomaterials at 1.58 V (*vs.* RHE) in the frequency range from10^5 to 10^{-2} s^{-1} with 0.005 V amplitude.

Catalyst	R_s (Ω)	R_{Ct} (Ω)	C_{dl} (μF)	R_P (Ω)	Q (m $Fs^{(a-1)}$)	Exp (n)
SL-$Co(OH)_2$	9.1	2	1.83	1276	0.36	0.86
α-$Co(OH)_2$	9.5	15	0.60	3014	0.89	0.85
β-$Co(OH)_2$	9.4	27	1.05	8637	0.43	0.75

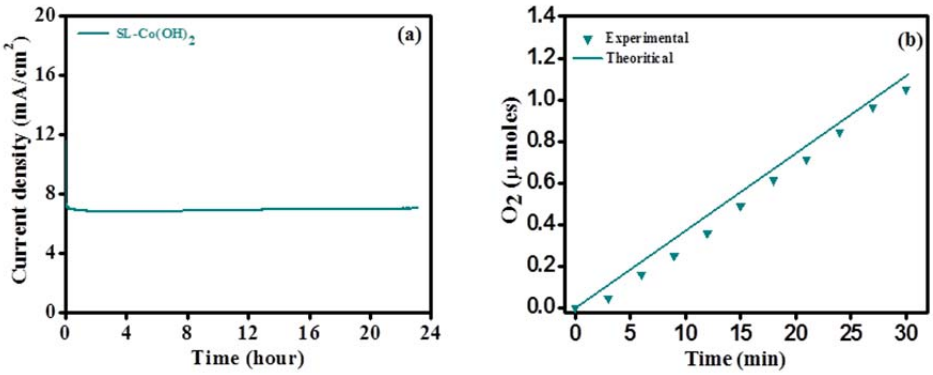

Figure S7: (a) Chronoamperogram showing the stability up to 23 h and (b) theoretical (cyan line) and experimental (cyan triangle) quantification of O_2 evolution of **SL-Co(OH)$_2$** at a constant potential of 1.58 V (*vs.* RHE) in 1 M NaOH during water oxidation.

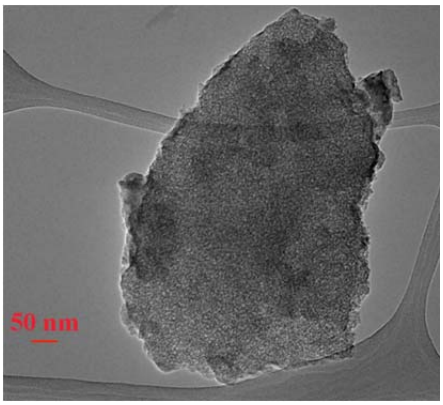

Figure S8: TEM image of **SL-Co(OH)$_2$** nanosheet after prolong chronoamperometry experiment at 1.58 V (*versus* RHE) in 1 M NaOH solution.

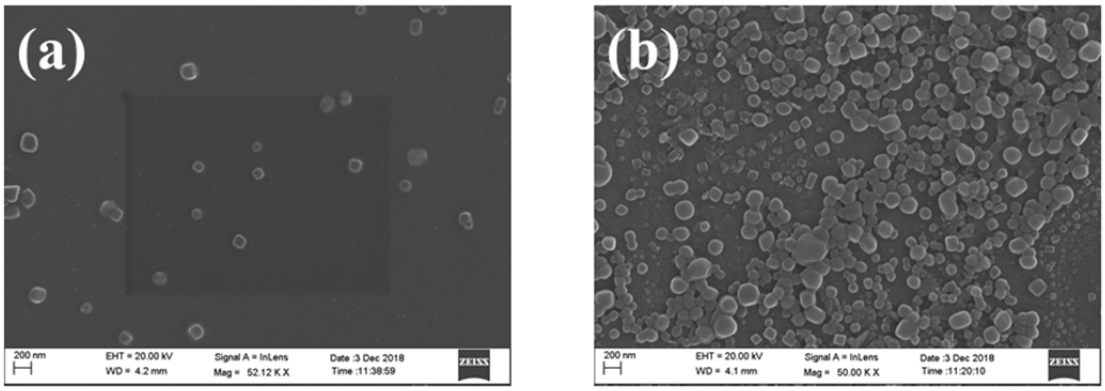

Figure S9: (a) and (b) Precatalysis and postcatalysis SEM images taken on silicon wafer after prolong chronoamperometry at 1.58 V (*versus* RHE) in 1 M NaOH solution. Precatalysis sample was prepared from a diluted concentration of **SL-Co(OH)$_2$** which resulted fewer sheets in the image.

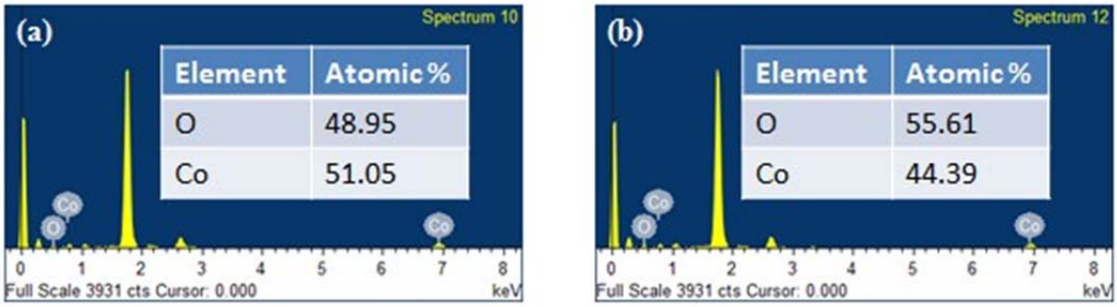

Figure S10: (a) and (b) Precatalysis and postcatalysis EDAX spectrum of **SL-Co(OH)$_2$** coated on silicon wafer after prolong chronoamperometry at 1.58 V (*versus* RHE) in 1 M NaOH solution

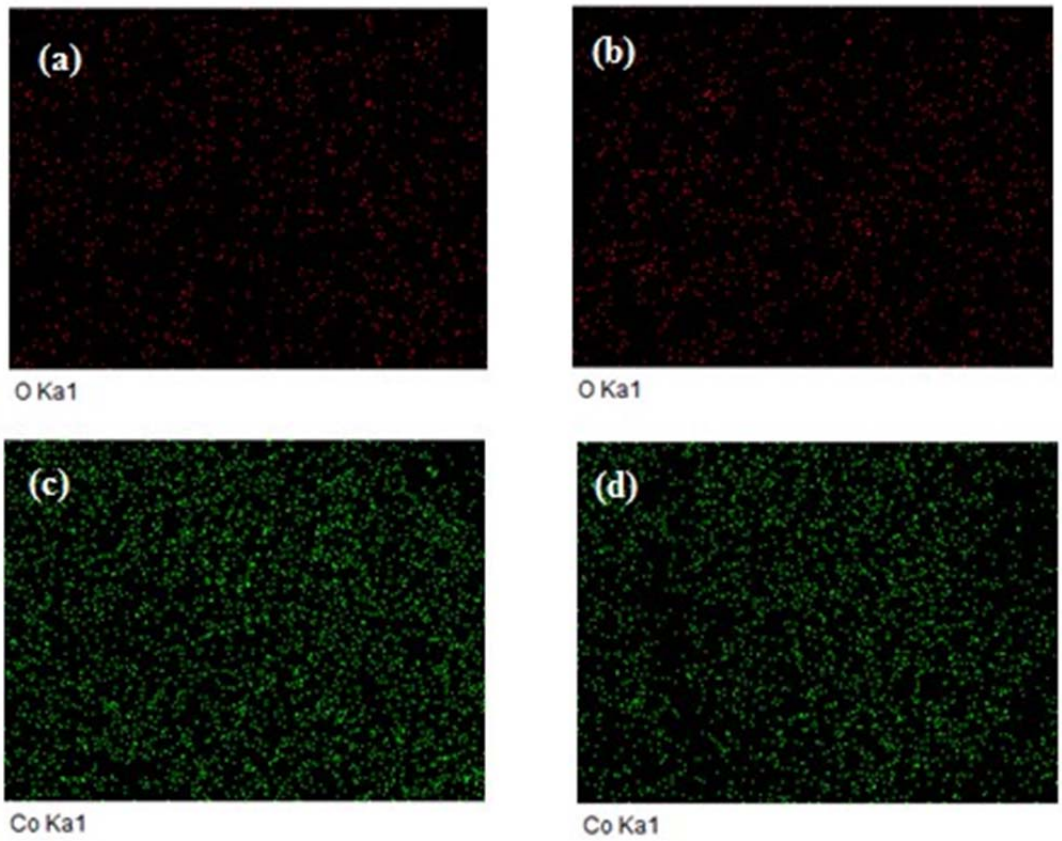

Figure S11: (a) and (b) precatalysis and postcatalysis oxygen atom elemental mapping whereas (c) and (d) are the precatalysis and postcatalysis corresponding cobalt atom elemental mapping of **SL-Co(OH)$_2$** after prolong chronoamperometry at 1.58 V (*versus* RHE) in 1 M NaOH solution.

Table S4: Literature reports of recently studied cobalt oxide based water oxidation electrocatalysts.

Catalyst	**TOF (s^{-1})**	**Mass activity @η=350 (j/m; A/g)**	**pH**	**Ref**
***SL*- Co(OH)$_2$**	***1.46× 10^{-1}***	***153.8***	***14***	***This work***
CoOOH nanosheets	9× 10^{-2} @300 mV	66.6 @300 mV	14	*Angew. Chem. Int. Ed.*, 2015, **54**, 8722
CoMn LDH nanosheets	0.9× 10^{-2} @300 mV	18.8 @300 mV	14	*J. Am.Chem. Soc.*, 2014, **136**, 16481
CoCo nanosheets	3× 10^{-3} @300 mV	-	14	*Nat. Commun.*, 2014, **5**, 4477
α Co(OH)$_2$ nanomesh	-	31.3@303 mV	14	*Chem. Commun.*, 2018, **54**, 4045
α Co(OH)$_2$ nanosheet	-	2.9@303 mV	14	*Chem. Commun.*, 2018, **54**, 4045

References:

1. K. Fan, H. Chen, Y. F. Ji, H. Huang, P. M. Claesson, Q. Daniel, B. Philippe, H. Rensmo, F. S. Li, Y. Luo and L. C. Sun, *Nat. Commun*., 2016, **7**, 11981-11989.
2. J. Saha, D. R. Chowdhury, P. Jash and A. Paul, *Chem.-Eur. J.* 2017, **23**, 12519-12526.
3. C. C. L. McCrory, S. H. Jung, J. C. Peters and T. F. Jaramillo, *J. Am. Chem. Soc.,* 2013, **135**, 16977-16987.
4. R. L. Doyle and M. E. G. Lyons, *Phys. Chem. Chem. Phys*., 2013, **15**, 5224-5237.
5. J. R. Swierk, S. Klaus, L. Trotochaud, A. T. Bell and T. D. Tilley, *J. Phys. Chem. C,* 2015, **119**, 19022-19029.
6. S. Bandyopadhyay, C. Singh, P. Jash, M. W. Hussain, A. Paul and A. Patra, *Chem. Commun*., 2018, **54**, 6796-6799.